Journal of Geophysical Research – Solid Earth

Supporting Information for

Probabilistic imaging of tsunamigenic seafloor deformation during the 2011 Tohoku-oki Earthquake

Junle Jiang[1,2*] and Mark Simons[1]

[1]Seismological Laboratory, California Institute of Technology, Pasadena, CA, USA
[2]Now at Institute of Geophysics and Planetary Physics, Scripps Institution of Oceanography, University of California San Diego, La Jolla, CA, USA.

*Corresponding author: Junle Jiang (junle@ucsd.edu)

Contents of this file

Text S1–S2
Figures S1–S4

Introduction

This Supplementary Information includes a summary on several theoretical dispersion relations for tsunami wave propagation (Text S1) and our methods to perturb waveforms based on the deviation in dispersion curves (Text S2). We also show the original and filtered tsunami waveforms used in the study (Fig. S1), theoretical dispersion curves (Fig. S2), travel paths between representative source-station pairs (Fig. S2), and the effect of different $\mathbf{C}_p$ on posterior data fit (Fig. S4).

Text S1. Frequency dispersion in tsunami propagation

Different approximations for the tsunami propagation model lead to different frequency dispersion characteristics. Based on analysis of the linear wave (Airy wave) theory, a typical frequency dispersion relation can be derived [e.g., *Kundu et al.*, 2012]. We express such relation in terms of the phase speed c as a function of the wavenumber k :

$$c = \sqrt{\frac{g \tanh(kh)}{k}}, \tag{S1}$$

where the wavenumber $k = 2\pi / \lambda$ with λ as the wavelength, g is the acceleration of gravity, and h is the water depth.

The shallow water approximation can be adopted when $h / \lambda \gg 1$, which is applicable for open-ocean propagation of tsunamis. Shallow-water waves have a constant phase speed with a given water depth and are hence non-dispersive:

$$c = \sqrt{hg}. \tag{S2}$$

The deep-water approximation is valid when $h\lambda \ll 1$. Deep-water waves are dispersive with the following dispersion relation:

$$c = \sqrt{\frac{g}{k}}. \tag{S3}$$

In the long-wave (long-period) limit, an additional mechanism modifies the dispersion relation due to the interaction between waves and the elastic substrate [e.g., *Watada*, 2013; *Tsai et al.*, 2013]:

$$c = \sqrt{\frac{g \tanh(kh)}{k}} \sqrt{1 - \frac{(1-\nu)\rho g}{\mu k}}, \tag{S4}$$

where ν is the Poisson's ratio and μ is the shear modulus. This effect can be ignored for small-scale problems. In the short-wave (short-period) limit, numerical approaches commonly adopt the Boussinesq approximation, in which the depth-dependence of horizontal velocities is accounted for and weakly dispersive waves are produced.

Here, we use NEOWAVE [*Yamazaki et al.*, 2009, 2011] which achieves the wave dispersion through non-hydrostatic terms, effectively reproducing dispersion relations that are closer to the theoretical predictions (Eq. S1) than the classical Boussinesq-type equations. Based on analysis of the linearized equations, the dispersion characteristics in NEOWAVE can be expressed as:

$$c = \sqrt{\frac{gh}{1 + \frac{1}{4}(kh)^2}}. \tag{S5}$$

Several dispersion relations above (Eq. S1, S4, and S5) clearly depend on the local water

depth h. Following the treatment of *Watada et al.* [2014], we normalize these relations by the long-wave phase speed $\sqrt{Hg}$ in Fig. S2. In reality, the "true" normalized dispersion curve could be complicated by nonlinear effects, and also be site- and path-dependent due to waves traveling through variable water depths.

Text S2. Perturbation of waveforms based on the dispersion relation

For tsunami modeling, deviation from the "true" normalized dispersion curve is an inevitable source of errors for the waveform prediction. We propose to explore the structure of $\mathbf{C}_\mathrm{p}$ for waveform misfits due to such kind of deviations. The empirical corrections of tsunami waveforms can be done with a given dispersion curve in the deterministic sense [e.g., *Yue et al.*, 2014]. Here, we carry out such waveform corrections in the stochastic sense based on a perturbation approach. We first generate random realizations of normalized dispersion curves with small deviations that follow a log-normal distribution centered on the curve associated with NEOWAVE (Eq. S5) and are bounded by the long-wave curve (Eq. S2). The synthetic waveform generated from a reference model is perturbed based on the deviation in dispersion characteristics for each random realization. For each frequency ω, the time delay $\Delta t(\omega)$ and phase delay $\phi(\omega)$ along the tsunami travel paths are:

$$\Delta t(\omega) = t_0(\omega) - t_\mathrm{p}(\omega) = \sum_i \left(\frac{p_i}{c_0(\omega, h_i)} - \frac{p_i}{c_\mathrm{p}(\omega, h_i)} \right), \tag{S6}$$

$$\phi(\omega) = -2\pi i \omega \Delta t(\omega), \tag{S7}$$

where c_0 and c_p are the reference and perturbed phase speed, respectively, both as a function of ω and local water depth h_i, and p_i is the discretized tsunami travel path.

With Eq. S6 and S7, we then make corrections to the tsunami Green's functions for each source-station pair at each frequency. We choose the ray path as the travel path between each source-station pair, which is calculated with a fast sweeping method based on an eikonal equation with long-wave propagation speeds dependent on the local water depth [*Zhao*, 2005]. In this case, the ray path is more realistic than the great-circle path due to the presence of deep-trench bathymetry which guides the propagation of tsunami (Fig. S3) [*Satake*, 1988].

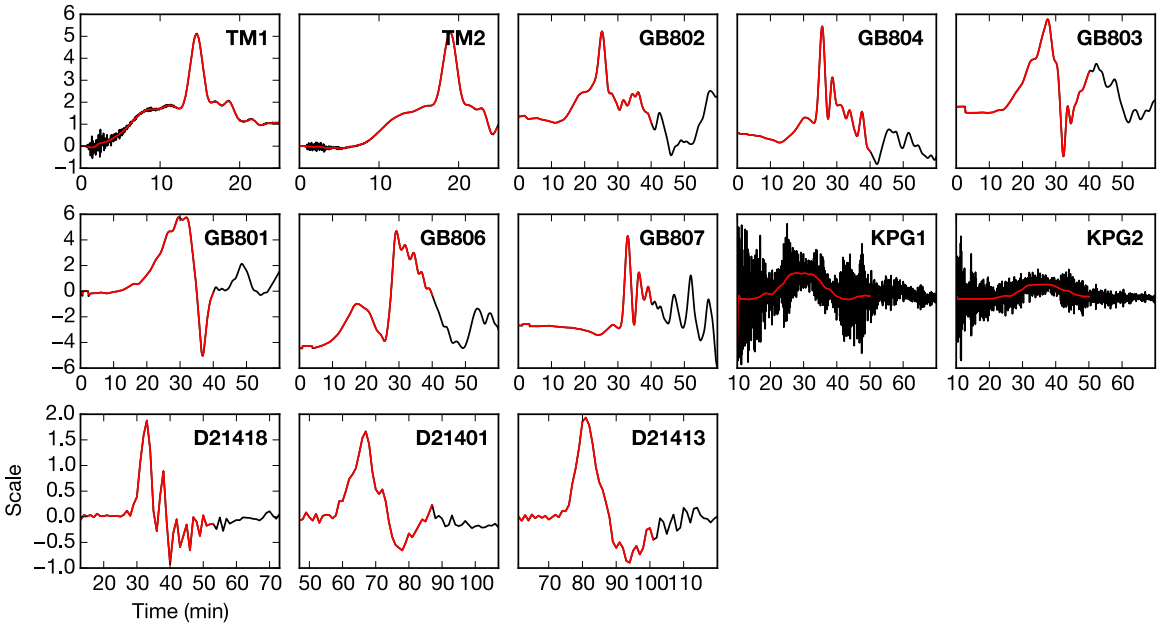

Figure S1. The original (black) and filtered (red) waveforms. Tsunami waveforms at 13 stations used in the study are lowpass-filtered at 2 mins for DARTs and 60 seconds for others.

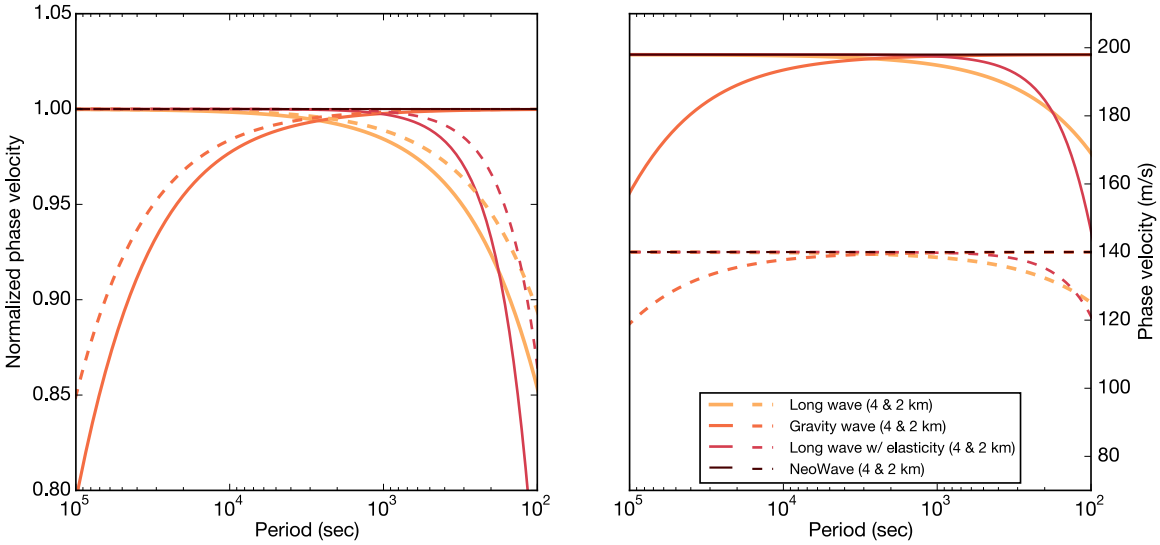

Figure S2. Frequency dispersion relations for tsunami propagation. (A) Phase speed normalized by the non-dispersive long-wave phase speed. (B) Absolute phase speed for cases with a water depth of 4 km (solid lines) and 2 km (dashed lines).

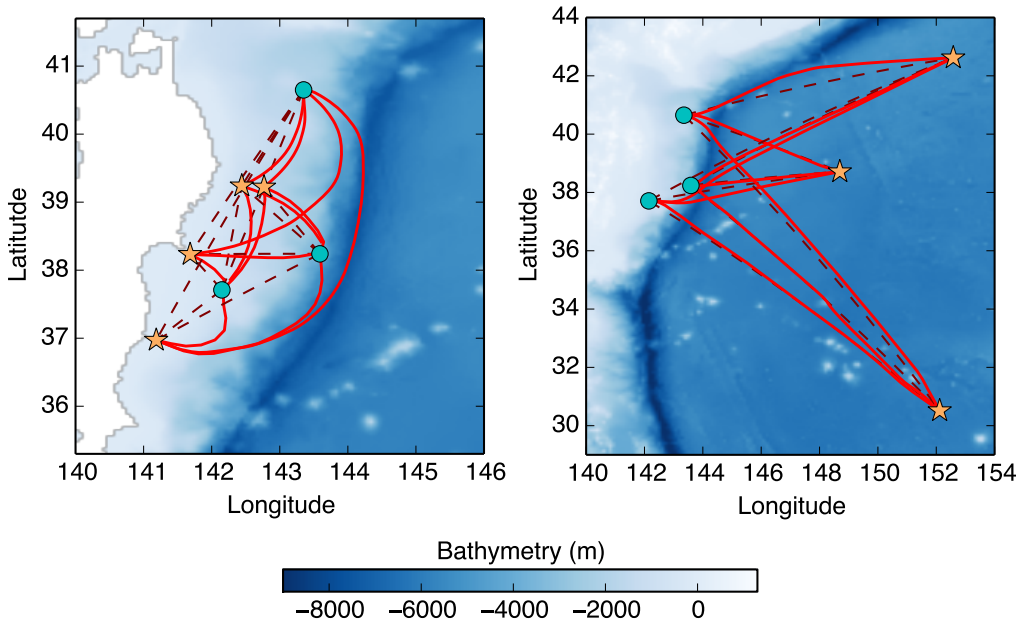

Figure S3. Travel paths between representative source-station pairs in tsunami propagation. (Left) Near-field stations and (Right) DART stations are represented by orange stars. Seafloor displacement sources are represented by blue circles. The ray path and great-circle path is indicated by solid and dashed lines, respectively.

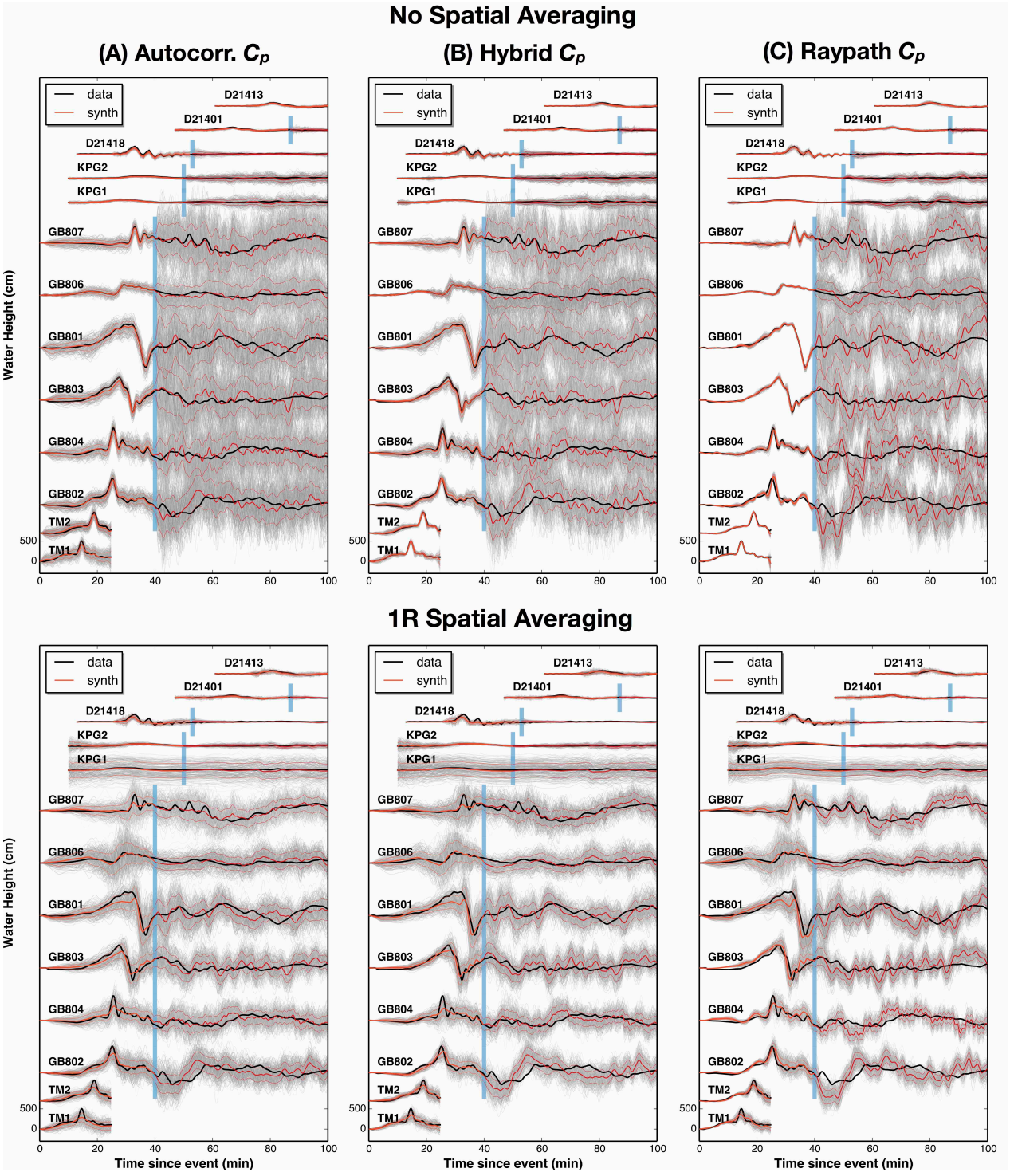

Figure S4. Effect of different model prediction errors $\mathbf{C}_p$ on posterior data fit. (Top row) solutions without spatial averaging. (Bottom row) Solutions with 1R spatial averaging.